AIAA Atmospheric Flight Mechanics Conference and Exhibit
11-14 August 2003, Austin, Texas

AIAA-2003-5609

ON THE USE OF RIGGING ANGLE AND CANOPY TILT FOR CONTROL OF A PARAFOIL AND PAYLOAD SYSTEM

Nathan Slegers* Mark Costello†
Department of Mechanical Engineering
Oregon State University
Corvallis, Oregon 97331

ABSTRACT

Controllable parafoil and payload aircraft are controlled with downward deflection of left and right parafoil brakes. Lateral control is obtained by differential deflection while longitudinal control is created by collective deflection of the left and right side parafoil brakes. The work reported considers an alternative method to control parafoil and payload air vehicles by tilting the parafoil canopy for lateral control and changing rigging angle for longitudinal control. Using a nonlinear 9 degree of freedom simulation model, it is shown that canopy tilt provides a powerful lateral control mechanism and rigging angle provides a viable longitudinal control mechanism.

NOMENCLATURE

x, y, z : Components of position vector of point C in an inertial frame.

ϕ_b, θ_b, ψ_b: Euler roll, pitch and yaw angles of payload.

ϕ_p, θ_p, ψ_p: Euler roll, pitch and yaw angles of parafoil.

$\dot{x}, \dot{y}, \dot{z}$: Components of velocity vector of point C in an inertial frame.

p_b, q_b, r_b: Components of angular velocity of payload in payload reference frame (b).

p_p, q_p, r_p: Components of angular velocity of parafoil in parafoil reference frame (p).

m_b, m_p : Mass of payload and parafoil.

I_b, I_p: Inertia matrix of payload and parafoil with respect to their mass centers.

I_F, I_M: Apparent mass force and moment coefficient matrices.

η : Rigging Angle.

τ : Canopy tilt.

T_p : Transformation matrix from inertial reference frame to parafoil reference frame.

T_b : Transformation matrix from inertial reference frame to payload reference frame.

F_A^b, F_A^p: Aerodynamic force components on payload and parafoil in their respective frames.

W_b, W_p: Weight payload and parafoil in their respective body frames.

M_C: Constraint moment components at Joint C.

S_c^a: Skew symmetric cross product operator distance vector from joint C to apparent mass center.

S_c^p: Skew symmetric cross product operator of distance vector from joint C to parafoil canopy mass center.

S_p^a: Skew symmetric cross product operator of distance vector from parafoil canopy mass center to apparent mass center.

S_ω^p: Skew symmetric cross product operator of parafoil angular velocity.

S_ω^b: Skew symmetric cross product operator of payload angular velocity.

INTRODUCTION

* Graduate Research Assistant, Department of Mechanical Engineering, Member AIAA.
† Associate Professor, Department of Mechanical Engineering, Member AIAA.

Compared to conventional fixed wing aircraft configurations, parafoil and payload air vehicles are compact and lightweight before launch, exhibit relatively long endurance, fly at low speed, and impact ground with low vertical velocity. For some air vehicle missions these characteristics are quite attractive, particularly for autonomous micro aircraft with long-term sensing or sensitive equipment delivery requirements.

The most common means to steer a parafoil is through deflection of right and left brakes on the parafoil. Iacomini and Cerimele [1] performed a detailed study on the turn performance of the X-38 parafoil and demonstrated extraction of lateral-directional aerodynamic coefficients from flight data. This data was inserted into an 8 degree-of-freedom parafoil and payload model for flight simulation validation. They noted that under certain conditions, adverse turn rates can be experienced, which they attributed to parafoil brake reflex. Jann [2] considered turn performance of the ALEX parafoil to support the development of a guided parafoil and payload system. Flight test data of parafoil turning angle was fit to a first order filter driven by brake deflection angle. Slegers and Costello [3] also considered turning performance of parafoil and payload systems and like Iacomini and Cerimele [1] found turning performance to be a complex function of canopy curvature, rigging angle, and brake deflection. They showed right and left parafoil brake deflection exhibit two basic modes of lateral control, namely, skid and roll steering, which generate lateral response in opposite directions. This control reversal is a complex function of rigging angle, canopy curvature, aerodynamic properties of the parafoil, as well as parafoil brake deflection magnitude and is particularly bothersome for autonomous systems that must automate control activity.

While left and right parafoil brake deflection is far and away the most common method of control, other control mechanisms for parafoil and payload systems are possible. For example, a method to affect turn control for a parafoil and payload system is to create an asymmetry in the suspension line lengths on both sides of the parafoil leading to a tilted canopy. Also, rigging angle has a powerful effect on the descent rate of the system. Large negative rigging angles lead to larger descent rates but are more stable at higher forward speed while rigging angles close to zero lead to lower descent rates but are less stable at high forward speed. For longitudinal control, the rigging angle can be dynamically changed in flight. While direct canopy tilt and dynamic rigging angle control appear on the surface to offer a viable control mechanism they have to date been unexplored in literature.

The work reported here explores the capability of canopy tilt for lateral control and dynamic rigging angle for longitudinal control of parafoil and payload systems. The paper begins with a description of a 9 degree-of-freedom simulation model used to make predictions and is followed by employing the model to predict control performance of a small autonomous parafoil and payload system. The effect of canopy tilt angle on turn rate, velocity, angle of attack, and glide rate is documented. Glide rate response for conventional symmetric brake deflection is contrasted against glide rate response with dynamic rigging angle.

PARAFOIL AND PAYLOAD SYSTEM MODEL

Figure 1 shows a schematic of the parafoil and payload system. With the exception of movable parafoil brakes, the parafoil canopy is considered to be a fixed shape once it has inflated. The combined system of the parafoil canopy and the payload is represented with a 9 degree-of-freedom (DOF) model, originally developed by Slegers and Costello [3]. The degrees-of-freedom include three inertial position components of the joint C as well as the three Euler orientation angles of the parafoil canopy and the payload. The canopy shape is modeled as a collection of panels oriented at fixed angle with respect to each other as shown in Figure 2. Connected to the outboard end panels are brakes that locally deflect the canopy downward. The parafoil canopy is connected to joint C by a rigid massless link from the mass center of the canopy. The payload is connected to joint C by a rigid massless link from the mass center of the payload. Both the parafoil and the payload are free to rotate about joint C but are constrained by the force and moment at the joint.

Kinematic equations of motion for the parafoil canopy and the payload are provided in Equations 1 through 3.

$$\begin{Bmatrix} \dot{x}_c \\ \dot{y}_c \\ \dot{z}_c \end{Bmatrix} = \begin{Bmatrix} u_c \\ v_c \\ w_c \end{Bmatrix} \tag{1}$$

$$\begin{Bmatrix} \dot{\phi}_b \\ \dot{\theta}_b \\ \dot{\psi}_b \end{Bmatrix} = \begin{bmatrix} 1 & s_{\phi_b} t_{\theta_b} & c_{\phi_b} t_{\theta_b} \\ 0 & c_{\phi_b} & -s_{\phi_b} \\ 0 & s_{\phi_b} / c_{\theta_b} & c_{\phi_b} / c_{\theta_b} \end{bmatrix} \begin{Bmatrix} p_b \\ q_b \\ r_b \end{Bmatrix} \tag{2}$$

$$\begin{Bmatrix} \dot{\phi}_p \\ \dot{\theta}_p \\ \dot{\psi}_p \end{Bmatrix} = \begin{bmatrix} 1 & s_{\phi_p} t_{\theta_p} & c_{\phi_p} t_{\theta_p} \\ 0 & c_{\phi_p} & -s_{\phi_p} \\ 0 & s_{\phi_p} / c_{\theta_p} & c_{\phi_p} / c_{\theta_p} \end{bmatrix} \begin{Bmatrix} p_p \\ q_p \\ r_p \end{Bmatrix} \quad (3)$$

The common shorthand notation for trigonometric functions is employed where $\sin(\alpha) \equiv s_\alpha$, $\cos(\alpha) \equiv s_\alpha$ and $\tan(\alpha) \equiv t_\alpha$.

The kinetic equations of motion are formed by first separating the system at the coupling joint, exposing the joint constraint force and moment acting on both bodies. The translational and rotational dynamics are inertially coupled because the position degrees of freedom of the system are the inertial position vector components of the coupling joint. The constraint force is a quantity of interest to monitor during the simulation so it is retained in the dynamic equations rather than being algebraically eliminated. Equation 4 represents the translational and rotational dynamic equations of both the parafoil and payload concatenated into matrix form.

$$\begin{bmatrix} -m_b S_c^b & 0 & m_b T_b & -T_b \\ 0 & -I_F S_c^a - m_p S_c^p & I_F T_p + m_p T_p & T_p \\ I_b & 0 & 0 & S_c^b T_b \\ 0 & I_M + I_p - S_p^a I_F S_c^a & S_p^a I_F T_p & -S_c^p T_p \end{bmatrix} \times \begin{Bmatrix} \dot{p}_b \\ \dot{q}_b \\ \dot{r}_b \\ \cdots \\ \dot{p}_p \\ \dot{q}_p \\ \dot{r}_p \\ \cdots \\ \ddot{x}_c \\ \ddot{y}_c \\ \ddot{z}_c \\ \cdots \\ F_{xc} \\ F_{yc} \\ F_{zc} \end{Bmatrix} = \begin{Bmatrix} \mathrm{B}_1 \\ \mathrm{B}_2 \\ \mathrm{B}_3 \\ \mathrm{B}_4 \end{Bmatrix} \quad (4)$$

The matrix in Equation 4 is a block 4 x 4 matrix where each element is a 3 x 3 matrix. Rows 1-3 in Equation 4 are forces acting on the payload mass center expressed in the payload frame and rows 7-9 are the moments about the payload mass center also in the payload frame. Rows 4-6 in Equation 4 are forces acting on the parafoil mass center expressed in the parafoil frame and rows 10-12 are the moments about the parafoil mass center also in the parafoil frame. Equations 5 through 8 provide the right hand side vector of Equation 4.

$$\mathrm{B}_1 = W_b + F_A^b - m_b S_\omega^b S_\omega^b \begin{Bmatrix} x_{cb} \\ y_{cb} \\ z_{cb} \end{Bmatrix} \quad (5)$$

$$\mathrm{B}_2 = W_p + F_A^p - I_F \dot{T}_p \begin{Bmatrix} \dot{x} \\ \dot{y} \\ \dot{z} \end{Bmatrix} - S_\omega^p I_F \begin{Bmatrix} u_A \\ v_A \\ w_A \end{Bmatrix} - m_p S_\omega^p S_\omega^p \begin{Bmatrix} x_{cp} \\ y_{cp} \\ z_{cp} \end{Bmatrix} \quad (6)$$

$$\mathrm{B}_3 = M_c - S_w^b I_b \begin{Bmatrix} p_b \\ q_b \\ r_b \end{Bmatrix} \quad (7)$$

$$\mathrm{B}_4 = M_A - T_p T_b^T M_c - S_\omega^p (I_p + I_M) \begin{Bmatrix} p_p \\ q_p \\ r_p \end{Bmatrix} - S_p^a I_F \dot{T}_p \begin{Bmatrix} \dot{x} \\ \dot{y} \\ \dot{z} \end{Bmatrix} - S_p^a S_\omega^p I_F \begin{Bmatrix} u_A \\ v_A \\ w_A \end{Bmatrix} \quad (8)$$

Equation 4 is solved using LU decomposition and the equations of motion described above are numerically integrated using a fourth order Runge-Kutta algorithm to simulate the motion of the system.

The focus of this paper is to analytically investigate the control response caused by direct canopy tilt and dynamic rigging angle. Canopy tilt is modeled by rotating the canopy about an outboard edge as shown in Figure 3. Canopy tilt can be implemented by mounting control lines along left and right outboard edges of the canopy. Dynamic rigging angle is modeled by rotating all parafoil canopy sections with respect to the massless link that connects the parafoil to point C. This is pictured in Figure 4. Dynamic rigging angle induces no change in brake deflection.

RESULTS

In order to explore the viability of canopy tilt and rigging angle as control mechanisms for parafoil and payload systems, the model described above is used to predict steady state control response

of a parafoil and payload aircraft for various canopy tilt, rigging angle, and parafoil brake settings. The parafoil and payload aircraft is identical to the configuration used by Slegers and Costello [4]. Physical parameters are listed in Tables 1 and 2. Aerodynamic coefficients were obtained from Slegers and Costello [4] and are listed in Table 3.

In all cases the system is launched at an altitude of 1000 *ft* with a level speed of 25 *ft/s* and is permitted to settle to a steady state condition with no control input. For the configuration under consideration this process takes 12 sec. At a prespecified time after launch, the appropriate control input is injected and held constant for the remainder of the flight. Steady turn rates are computed for canopy tilt angles from 0.0 to 3.0 *deg* in increments of 0.5 *deg* and right brake deflection from 0.0 to 2.875 *in* by increments of 0.0479 *in* and are plotted in Figure 5. Canopy tilt is considered positive when the right outboard edge is moved lower. Increasing amounts of pure right brake deflection produce increasingly more negative turn rates with a turn rate of –177 *deg/s* reached for a full right brake of 2.875 *in*. Increasing amounts of pure canopy tilt produces larger positive turn rates with a maximum of 215 *deg/s* reached at 3 *deg* of canopy tilt. The extreme cases of large brake deflections with no canopy tilt and large canopy tilt with no brake deflection produce extremely large turn rates. Thus, canopy tilt provides a powerful mechanism for parafoil and payload turning.

Large positive turn rates predicted by pure canopy tilt are a result of the total canopy roll sensitivity to canopy tilt. Figure 6 shows the resulting canopy roll induced by canopy tilt. Total canopy roll quickly becomes large and reaches a maximum of 61 deg at 1.5 deg of canopy tilt before slightly decreasing. Canopy tilt is amplified and results in larger overall roll angles of the parafoil. Figure 7 shows the amplification factor of a canopy tilt input. The largest amplification factor of 83 occurs at 0.55 deg of canopy tilt. The amplification of canopy tilt into larger total canopy roll explains predicted sensitivity to small canopy tilt.

Commonly parafoils exhibit positive turn rates when the right brake is deflected fully, opposite that predicted by a pure right brake in Figure 5. If right brake and positive canopy tilt are coupled so that deflecting the right brake also pulls the right outboard edge down, turn response dramatically changes from pure right brake response. A solid line in Figure 5 shows the intersection of the control response surface with zero turn response plane. Brake deflection causes both positive and negative turn rates depending on the amount of canopy tilt associated. Parafoil canopies are highly flexible membranes even when inflated, so that deflection of a parafoil brake on one side also tilts the canopy down on that side. The amount of canopy tilt induced by brake deflection is strongly dependent on connection of the control lines to the canopy and the number of lines on the canopy. Thus, turn performance of the parafoil and payload systems is caused by the difference of the two powerful turning mechanisms.

For longitudinal control, in flight modification of the glide slope and total velocity of the parafoil and payload system is also desirable. Commonly, speed and glide slope is controlled by deflecting both brakes simultaneously. Dynamically changing rigging angle in flight also controls glide slope and speed. Figure 8 shows predicted glide slopes from symmetric brake deflection and rigging angle. Glide slope is reduced from 0.328 to under 0.248 over the range of symmetric brake deflection while reducing rigging angle from -13.5 *deg* to -2 *deg* only achieves a reduction in glide slope from 0.331 to .307. Figure 9 shows that rigging angle deflection over the range of –13.5 *deg* to –2 *deg* yields a reduction in total velocity from 23.9 *ft/s* to 19.7 *ft/s* and from symmetric brake deflection a reduction from 22.8 *ft/s* to 21.1 *ft/s*. Figure 10 shows that rigging angle deflection effectively increases angle of attack thus reducing overall velocity of the system. Symmetric brake deflection only slightly alters angle of attack. Thus, decreased glide slope is not from increasing the angle of attack like dynamic rigging but instead from increasing of lift thus reducing the angle of attack. Rigging angle and symmetric brake deflections both reduce glide slope and total velocity of a parafoil and payload system but use different mechanisms. Rigging angle modification can effectively reduce the total velocity of the parafoil system and reduce the glide slope resulting in a viable longitudinal control mechanism.

CONCLUSIONS

Due to the fact that the parafoil canopy is a flexible membrane, deflection of the control arms on one side of the parafoil may also create tilt of the canopy. Both these effects combine together to form the overall turning response. The parafoil and payload system discussed exhibits high lateral sensitivity to subtle canopy tilting. The high sensitivity to canopy tilt illustrates the importance of design parameters that alter the flexibility of the canopy namely suspension line quantity and arrangement and control line configuration. Canopy tilting can be exploited to eliminate conventional parafoil brakes for lateral direction control.

Symmetric brake deflection and rigging angle modification both demonstrate the ability to effectively alter glide slope and total velocity of the system but in different methods. Rigging angle modification alters the glide slope and total velocity by largely altering the aerodynamic angle of attack while symmetric brake deflection increases the lift only slightly increasing the angle of attack. In comparison symmetric brake deflections are more effective in altering the glide slopes and rigging angle modifications more effectively alter the total velocity.

Conventional parafoil brakes for lateral and longitudinal control could be replaced by a combination of canopy tilting for lateral control and rigging angle modification for longitudinal control. A benefit of this alternate control method is the possibility of decoupling the lateral and longitudinal control mechanisms.

REFERENCES

[1] Iacomini, C.S., Cerimele, C.J., "Lateral-Directional Aerodynamics from a Large Scale Parafoil Test Program," AIAA Paper 99-1731.

[2] Jann, T., "Aerodynamic Model Identification and GNC Design for the Parafoil-Load- System ALEX," AIAA Paper 2001-2015.

[3] Slegers, N., Costello M., "Aspects of Control for a Parafoil and Payload System," Journal of Guidance, Control and Dynamics, Vol. 26, No. 6, December 2003

[4] Slegers, N., Costello M., "Comparison of Measured and Simulated Motion of a Controllable Parafoil and Payload System," AIAA Paper 2003-5611, 2003

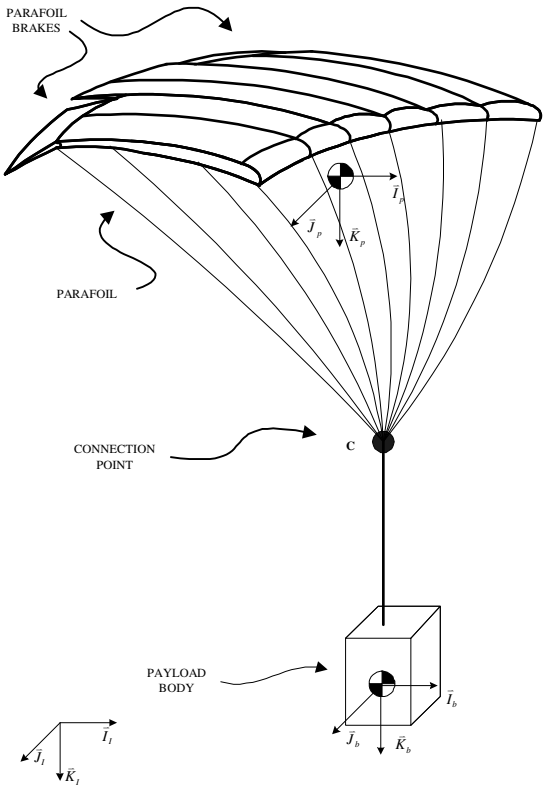

Figure 1- Parafoil and Payload

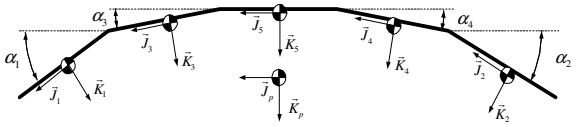

Figure 2 – Parafoil Canopy Geometry

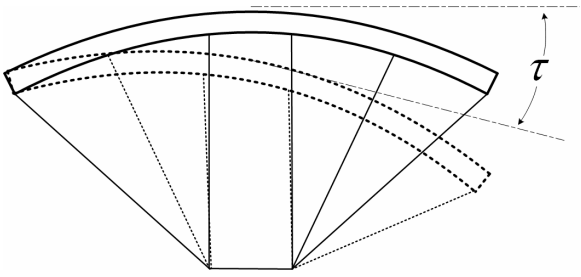

Figure 3 – Canopy Tilting

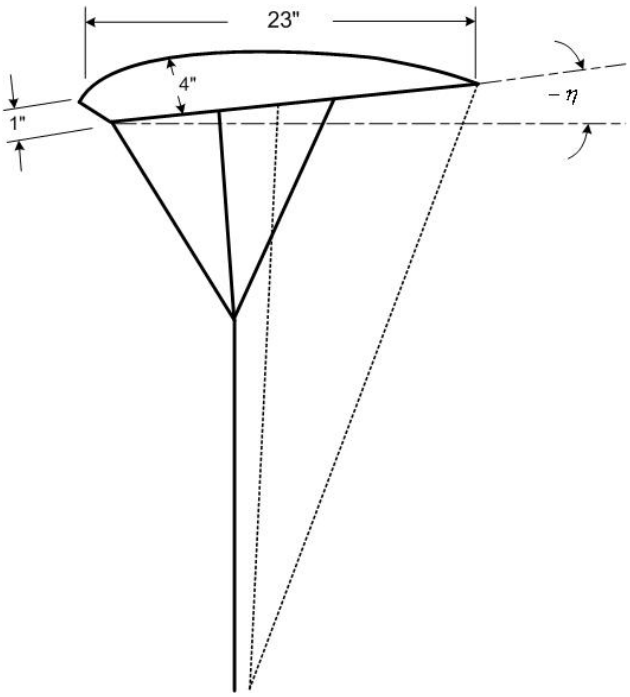

Figure 4 – Angle of Incidence

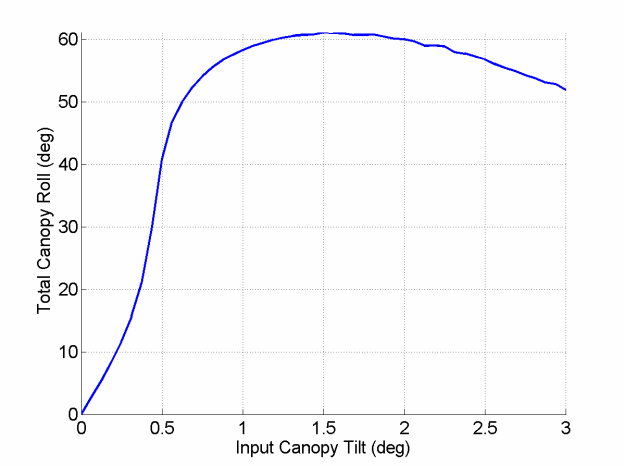

Figure 6 – Canopy Roll Induction By Tilt

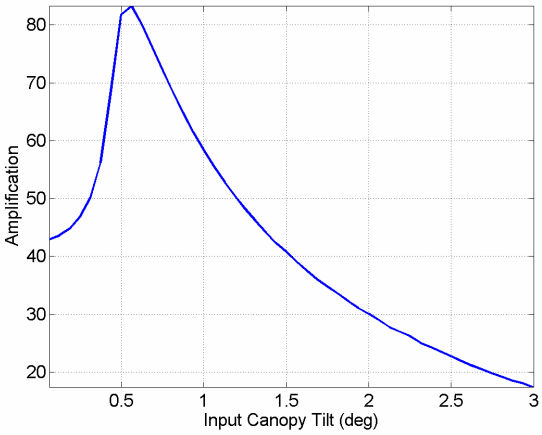

Figure 7 – Roll Amplification

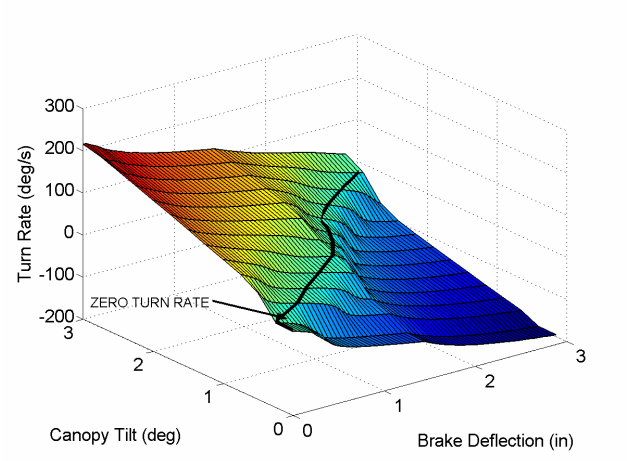

Figure 5 – Turn Response Brake Deflection on Right Side and Positive Canopy tilt

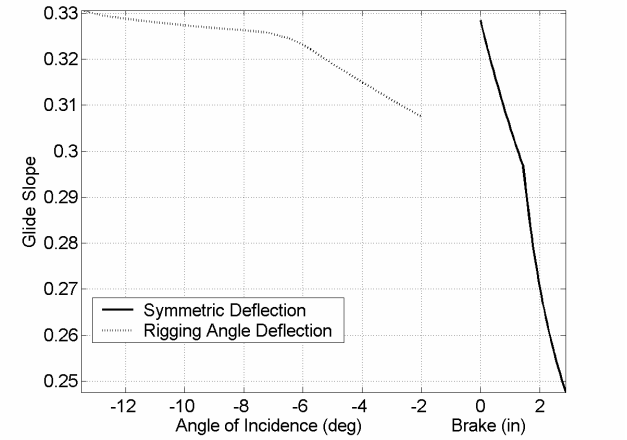

Figure 8 – Glide Slope

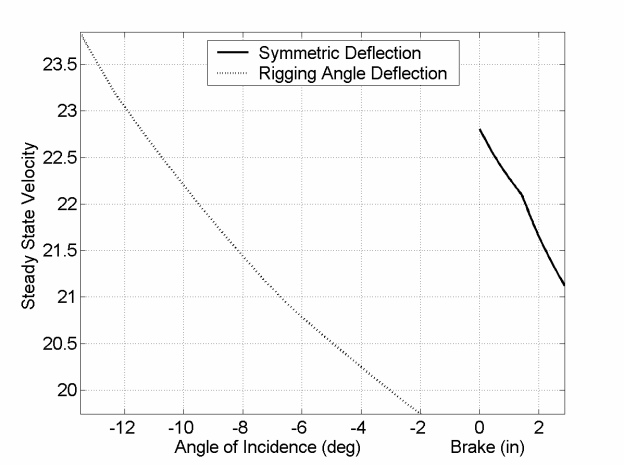

Figure 9 – Steady State Total Velocity

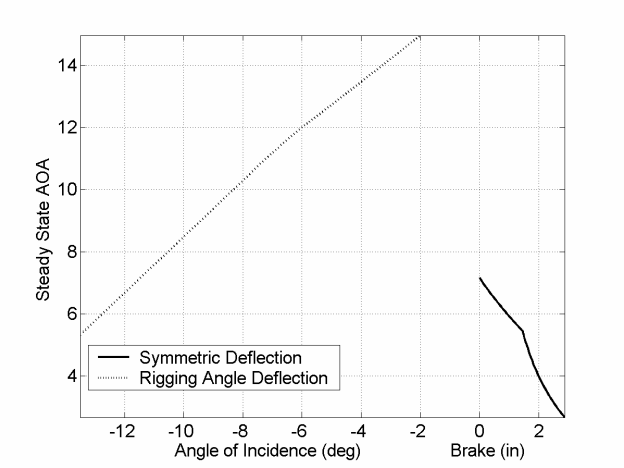

Figure 10 – Steady State Angle of Attack

Table 1 – Physical Parameters

Parameter	Value	Description
n	5	Number of Panels
α_1	25 deg	Panel 1 Angle
α_2	-25 deg	Panel 2 Angle
α_3	20 deg	Panel 3 Angle
α_4	-20 deg	Panel 4 Angle
α_5	0 deg	Panel 5 Angle
η	-11.5 deg	Incidence Angle
S	2.61 ft^2	Panel Area
t	4 in	Panel thickness
w_p	0.45 lbf	Parafoil Weight
w_b	4.1 lbf	Payload Weight

Table 2 – Apparent Mass Coefficients

Coefficient	Value
A	0.0019
B	0.00021
C	0.044
I_A	0.11
I_B	0.010
I_C	0.0070

Table 3 – Estimated Aerodynamic Coefficients

Parameter	Flight 1	Flight 3	Flight 5
α (deg)	7.4	5.7	2.8
$C_L(\alpha_T)$	.571	.757	1.08
$C_D(\alpha_T)$	.168	.169	.161